



## Ultrafast valley polarization of graphene nanorings

Ahmal Jawad Zafar , Aranyo Mitra , and Vadym Apalkov

*Department of Physics and Astronomy, Georgia State University, Atlanta, Georgia 30303, USA*



(Received 6 July 2022; revised 22 September 2022; accepted 11 October 2022; published 25 October 2022)

We study theoretically electron dynamics of a graphene nanoring placed in the field of an ultrashort optical pulse. We describe the graphene nanoring within an effective model with infinite mass boundary conditions. For an optical pulse with a duration of just a few femtoseconds, the electron dynamics is coherent and is described by a time-dependent Schrödinger equation. If the optical pulse is circularly polarized, then two valleys of graphene are populated differently, resulting in a finite valley polarization of the system after the pulse. Such a valley polarization is a unique property of graphene nanoscale systems, while for a graphene monolayer, a circularly polarized pulse does not produce any valley polarization. The valley polarization of the graphene nanoring depends on parameters of the system, such as inner and outer radii. With the system's size increasing, the valley polarization monotonically decreases, converging to its zero value for the infinite graphene monolayer.

DOI: [10.1103/PhysRevB.106.155147](https://doi.org/10.1103/PhysRevB.106.155147)

### I. INTRODUCTION

Graphene systems, such as graphene monolayer, bilayer, and multilayers, have been extensively studied both theoretically and experimentally over the last few decades [1–7]. The interest in such systems is related to their unique transport, optical, and topological properties. At the same time, they are very simple systems based on a single element, a carbon atom.

A graphene monolayer is a single layer of carbon atoms which form a honeycomb crystal structure with two inequivalent sublattices, say,  $A$  and  $B$ . One of the unique features of the graphene monolayer is its low-energy relativistic dispersion of a Dirac type [1]. The corresponding electron states are chiral, where the chirality is related to the pseudospin originating from the two graphene sublattices. The chiral nature of electron states brings such unique effects as Klein tunneling, strong suppression of backscattering, and localization [4].

Another attractive property of the graphene monolayer is the existence of two valleys in its reciprocal space. The valleys are located at the  $K$  and  $K'$  points at the vertices of the hexagonal first Brillouin zone of graphene [5]. The energy spectra at these points are gapless and relativistic; that is, they are the Dirac points. The time-reversal operator connects the  $K$  and  $K'$  valleys. Here, the time-reversal symmetry is the symmetry of the graphene monolayer. Electrons in graphene also have nontrivial local topological properties. Namely, while the net topological charge (Chern number) for the whole Brillouin zone of graphene is zero, the topological charges at the  $K$  and  $K'$  points are 1 and  $-1$ , respectively [8].

The existence of the two valleys in graphene opens a possible application of graphene in valleytronics [9–11], where the valley degree of freedom can be used for information storage and quantum computer applications. The two valleys in graphene are well separated in the reciprocal space, and an intervalley scattering is strongly suppressed for a smooth scattering potential. In this relation, there is a problem with how

to generate and manipulate valley polarization in graphene. Here, the valley polarization is determined by the different valley populations of the system. To generate the valley polarization in graphene, the time-reversal symmetry should be broken. This can be done, for example, by an incident circularly polarized pulse. If such a pulse is ultrashort with just a few oscillations of the field, then it will allow controlling the valley degree of freedom on the femtosecond timescale. In Refs. [12–14], interactions of graphenelike systems with a circularly polarized short and ultrastrong pulse were considered. It was found that such a pulse can induce large final valley polarization, but to have such a valley polarization, the inversion symmetry of graphene should be broken. This means that graphene should have a finite band gap. Under such a condition, the valley polarization is generated due to the effect of topological resonance [13–15]. The topological resonance is a cancellation of a dynamic phase by a topological phase, which is accumulated during a strong optical pulse. In pristine graphene that has a zero band gap, the topological phase, which consists of a geometric phase (Berry phase) and a phase of an interband dipole matrix element (non-Abelian Berry connection), is effectively zero, so no topological resonance can be observed in such a system. In graphene systems with broken inversion symmetry, the topological phase is proportional to the band gap and has different signs at the two valleys, which results in the valley-dependent topological resonance [15]. The inversion symmetry is broken in graphenelike materials with two sublattices occupied by different atoms, e.g., transition-metal dichalcogenides (TMDCs) [16–18], and in silicene/germanene, which has a buckled hexagonal shape and in which the perpendicular electric field breaks the inversion symmetry [19–21]. In graphene, a small band gap can also be opened if it is placed on different types of substrates, e.g., on SiC [22,23]. The finite valley polarization of TMDC monolayers placed in an ultrashort circularly polarized pulse was predicted theoretically in Ref. [13].

Here, we propose another method to generate ultrafast valley polarization in graphene materials. We consider a nanoflake of graphene. The example of such a system is a graphene quantum dot (QD) [24–26]. For such a system, a translational symmetry is broken, and the band gap is opened due to a dimensional quantization. Quantum dots and other types of nanosize systems are zero-dimensional; that is, electrons are confined in all spatial directions and occupy spectrally sharp energy levels like those found in atoms [27–29]. Similar to conventional atoms, the properties of QDs, which are also called artificial atoms, are governed by the Hund's rule [29,30], which determines electron occupations of degenerate QD energy levels; the Coulomb blockade [31], which is a manifestation of electron-electron interactions within the QD; and the Kondo effect [32], which is related to electron spin.

The QDs are between a few nanometers and a few microns in size. Due to such a tiny scale, the QDs can be occupied by just a few electrons, which allows controlling and optimizing QD-based nanoscale devices. The QDs also show superior transport and optical properties with many applications in different fields of science, such as semiconductor lasers [33], quantum computers [34], biomedical systems [35], and light-energy conversion [36,37].

In the present paper, we consider graphene nanosize systems with a special shape. Namely, we consider graphene nanorings. Similar to QDs, nanorings have discrete energy spectra with unique transport and optical properties. Graphene nanorings have two parameters, the inner and outer radii of the ring, which can be used to tune their properties. Below, to describe an electron system of a graphene nanoring, we use an effective model which is applied separately to the  $K$  and  $K'$  valleys of graphene. Interaction of the graphene nanoring with an ultrashort circularly polarized optical pulse should generate different conduction band populations of the two valleys, resulting in finite final valley polarization of the system.

This paper is organized as follows. In Sec. II we introduce the model and the main equations. We also define the graphene nanoring and the optical pulse shape considered in our calculations. In Sec. III, we present our numerical results for the valley polarization of the graphene nanoring. The concluding remarks are given in Sec. IV.

## II. MODEL AND MAIN EQUATIONS

We consider a graphene nanoring with inner radius  $R_{\text{in}}$  and outer radius  $R_{\text{out}}$ . We describe graphene within an effective low-energy model with the Hamiltonian being of a Dirac type, which for a graphene nanoring takes the following form:

$$\mathcal{H}_0^{(\xi)} = \frac{\gamma}{\hbar} (\sigma_x p_x + \xi \sigma_y p_y) + V(\mathbf{r}), \quad (1)$$

where  $\sigma_x$  and  $\sigma_y$  are the Pauli matrices,  $p_x = -i\hbar\nabla_x$ ,  $p_y = -i\hbar\nabla_y$ , and  $\gamma = \sqrt{3}a_0\gamma_0/2$  is the band parameter with the lattice constant  $a_0 = 0.142$  nm and the nearest neighbor hopping integral  $\gamma_0 = 3.03$  eV. Here,  $\xi$  is the valley parameter, which is  $+1$  for the  $K$  valley and  $-1$  for the  $K'$  valley. Since the spin-orbit interaction is very weak in graphene, the Hamiltonian (1) is written only for one spin component, e.g., spin up. Thus,

each energy level calculated below has an extra double spin degeneracy. The confinement potential  $V(\mathbf{r})$  is of the mass form,  $V(\mathbf{r}) = \Delta(\mathbf{r})\sigma_z$ , where  $\sigma_z$  is the Pauli matrix. Here,  $\Delta(\mathbf{r})$  is zero inside the nanoring and  $\Delta(r) \rightarrow \infty$  outside. Such a profile of the confinement potential introduces infinite mass boundary conditions [38–41] at the boundary of the nanoring. Although the properties of graphene nanorings depend on the type of their edges, e.g., zigzag or armchair edges, the infinite boundary conditions can be a good approximation for graphene nanostructures that are etched out of graphene sheets by lithography (see Refs. [41–45]).

Because the nanoring has cylindrical symmetry, its electron states are characterized by a  $z$  component of angular momentum  $m$ , i.e., a magnetic quantum number, which takes half-integer values,  $m = \pm 1/2, \pm 3/2, \pm 5/2, \dots$ . The corresponding eigenfunctions of Hamiltonian (1) can be written for the valley  $\xi$  in the following form:

$$\psi^{(\xi)}(r, \theta) = e^{i(m-\xi/2)\theta} \begin{pmatrix} \chi_1^{(\xi)}(r) \\ e^{i\xi\theta} \chi_2^{(\xi)}(r) \end{pmatrix}, \quad (2)$$

where  $r$  and  $\theta$  are polar coordinates. Substituting the form of the wave function (2) into the eigenvalue equation  $H_0\psi^{(\xi)}(r, \theta) = E\psi^{(\xi)}(r, \theta)$ , we obtain the following system of equations for functions  $\chi_1^{(\xi)}(r)$  and  $\chi_2^{(\xi)}(r)$ :

$$\nabla_r \chi_1^{(\xi)}(r) - \frac{(m-\xi/2)}{r} \chi_1^{(\xi)}(r) = \frac{iE}{\gamma} \chi_2^{(\xi)}(r), \quad (3)$$

$$\nabla_r \chi_2^{(\xi)}(r) + \frac{(m+\xi/2)}{r} \chi_2^{(\xi)}(r) = \frac{iE}{\gamma} \chi_1^{(\xi)}(r). \quad (4)$$

Then substituting  $\chi_2^{(\xi)}$  from Eq. (3) into Eq. (4), we obtain the differential equation for  $\chi_1^{(\xi)}(r)$ ,

$$\nabla_r^2 \chi_1^{(\xi)}(r) + \frac{1}{r} \nabla_r \chi_1^{(\xi)}(r) - \left( \frac{(m+\xi/2)^2}{r^2} - \frac{E^2}{\gamma^2} \right) \chi_1^{(\xi)}(r) = 0. \quad (5)$$

The above equation is the Bessel equation, and its solution can be expressed as a superposition of the Bessel and Neumann functions,

$$\chi_1^{(\xi)}(r) = C_1^{(\xi)} J_{m-\xi/2} \left( \varepsilon \frac{r}{R_{\text{out}}} \right) + C_2^{(\xi)} N_{m-\xi/2} \left( \varepsilon \frac{r}{R_{\text{out}}} \right), \quad (6)$$

where  $J_n(x)$  is the Bessel function of the first kind of order  $n$ ,  $N_n(x)$  is the Neumann function of order  $n$ , and  $\varepsilon = \frac{R_{\text{out}} E}{\gamma}$ . Here,  $C_1^{(\xi)}$  and  $C_2^{(\xi)}$  are constants. From Eq. (3) we can also find the second component of the wave function,

$$\chi_2^{(\xi)}(r) = iC_1^{(\xi)} J_{m+\xi/2} \left( \varepsilon \frac{r}{R_{\text{out}}} \right) + iC_2^{(\xi)} N_{m+\xi/2} \left( \varepsilon \frac{r}{R_{\text{out}}} \right). \quad (7)$$

The energy spectrum of the nanoring is obtained from the infinite mass boundary conditions, which are introduced through the following expression [38]:

$$\lim_{r \rightarrow \mathbf{R}} \chi_1^{(\xi)}(r) = i\xi \lim_{r \rightarrow \mathbf{R}} \chi_2^{(\xi)}(r), \quad (8)$$

where  $\mathbf{R}$  is the boundary of the nanoring, i.e.,  $r = R_{\text{in}}$  and  $r = R_{\text{out}}$ . Substituting Eqs. (6) and (7) into Eq. (8), we obtain

the equation for the eigenenergies of the system:

$$\frac{\xi N_{m+\xi/2}(\varepsilon R_{\text{in}}/R_{\text{out}}) + N_{m-\xi/2}(\varepsilon R_{\text{in}}/R_{\text{out}})}{\xi J_{m-\xi/2}(\varepsilon R_{\text{in}}/R_{\text{out}}) + J_{m+\xi/2}(\varepsilon R_{\text{in}}/R_{\text{out}})} = \frac{\xi N_{m+\xi/2}(\varepsilon) + N_{m-\xi/2}(\varepsilon)}{\xi J_{m-\xi/2}(\varepsilon) + J_{m+\xi/2}(\varepsilon)}. \quad (9)$$

With the known wave functions, the dipole matrix elements between states  $i$  and  $j$  can be calculated from the following expression:

$$\mathbf{D}_{ij}^{(\xi)} = \langle \psi_j^{(\xi)} | e\mathbf{r} | \psi_i^{(\xi)} \rangle. \quad (10)$$

Substituting Eq. (2) for the wave functions in terms of  $\chi_1$  and  $\chi_2$ , we obtain the  $x$  and  $y$  components of the dipole matrix elements

$$D_{x,ij}^{(\xi)} = e\pi [\delta(m_i, m_j - 1) + \delta(m_i, m_j + 1)] \times \int_{r_{\text{in}}}^{r_{\text{out}}} [\chi_{1,j}^{(\xi)*}(r)\chi_{1,i}^{(\xi)}(r) + \chi_{2,j}^{(\xi)*}(r)\chi_{2,i}^{(\xi)}(r)] r^2 dr \quad (11)$$

and

$$D_{y,ij}^{(\xi)}(r, \theta) = -ie\pi [\delta(m_i, m_j - 1) - \delta(m_i, m_j + 1)] \times \int_{r_{\text{in}}}^{r_{\text{out}}} [\chi_{1,j}^{(\xi)*}(r)\chi_{1,i}^{(\xi)}(r) + \chi_{2,j}^{(\xi)*}(r)\chi_{2,i}^{(\xi)}(r)] r^2 dr. \quad (12)$$

Here,  $m_i$  and  $m_j$  are magnetic quantum numbers of the corresponding states  $i$  and  $j$ . As expected, the dipole transitions have selection rule  $m_i = m_j \pm 1$ .

Now we place the graphene nanoring in the field of an optical pulse. The corresponding electron dynamics is described by the time-dependent Hamiltonian of the form

$$\mathcal{H}^{(\xi)}(t) = \mathcal{H}_0^{(\xi)} + e\mathbf{F}(t) \cdot \mathbf{r}, \quad (13)$$

where  $\mathbf{F}(t)$  is the pulse's electric field. Below we consider only a circularly polarized optical pulse. Such a pulse breaks the inversion symmetry of the system, which can result in a finite final valley polarization of the system. The profile of the electric field of the circularly polarized pulse is given by the following expression:

$$F_x(t) = F_0 e^{-u^2} (1 - 2u^2), \quad (14)$$

$$F_y(t) = F_0 e^{-u^2} (2u), \quad (15)$$

where  $u = t/\tau$  and time parameter  $\tau$  determines the pulse's duration and frequency. Below, the main results are shown for  $\tau = 1$  fs, i.e., the frequency of the pulse  $\approx 1$  eV. Here, we consider only one oscillation of the field, addressing the problem of ultrafast control of the valley degree of freedom. Thus, we consider the case when valley polarization can be generated by just a single oscillation of the optical pulse. Under this condition, only one parameter,  $\tau$ , characterizes the pulse's duration and frequency. We assume that the pulse duration, around 6 fs, is less than the characteristic relaxation times of the nanoring. In this case, the electron dynamics within the graphene nanoring is described by the time-dependent Schrödinger equation,

$$i\hbar \frac{d\Psi^{(\xi)}(t)}{dt} = \mathcal{H}^{(\xi)}(t)\Psi^{(\xi)}(t). \quad (16)$$

We expand a solution of Eq. (16) in the basis of single-particle states (2)  $\psi_i$ ,

$$\Psi^{(\xi)}(t) = \sum_{j=1}^N \beta_j^{(\xi)}(t) \psi_j^{(\xi)} e^{-\frac{i}{\hbar} E_j t}, \quad (17)$$

with the time-dependent expansion coefficients  $\beta_i^{(\xi)}(t)$ . Strictly speaking, the energy spectrum of the graphene nanoring, within the effective low-energy model, consists of an infinite number of levels in both the conduction and valence bands. In our approach, we consider a finite number  $N$  of nanoring levels, the energies of which are in the interval from  $-2$  eV to  $2$  eV. The number of such levels depends on the size of the nanoring.

The intensity of the optical pulse we consider below is small enough that the pulse's electric field does not mix the states of different valleys. The amplitude of the pulse, which can result in the coupling of the valleys, can be estimated from the condition that, during the pulse, an electron is transferred between the two valleys, i.e., over the distance of  $4\pi/3\sqrt{3}a_0$ . The corresponding field amplitude can be estimated as  $F_0 \approx 4\pi\hbar/3\sqrt{3}\tau a_0 \approx 1.1$  V/Å. Below, we consider optical pulses with amplitudes less than  $0.5$  V/Å.

The coefficients  $\beta_i(t)$  in Eq. (17) satisfy the following system of differential equations:

$$\frac{d\beta_k^{(\xi)}}{dt} = -\frac{i}{\hbar} \sum_{j=1}^N \mathbf{F}(t) \cdot \mathbf{D}_{kj}^{(\xi)}(t) \beta_j^{(\xi)} e^{-\frac{i}{\hbar}(E_j - E_k)t}. \quad (18)$$

We solve the system of equations (18) numerically with the conditions that all the valence band (VB) states are initially occupied and all the conduction band (CB) states are empty. The equations are solved using the Runge-Kutta method, where the initial time is  $-3\tau$  and the final time is  $3\tau$ . From the solution of Eq. (18) we obtain the final populations of the CB levels, i.e., the populations after the pulse. We find the CB populations for both the  $K$  and  $K'$  valleys,

$$\mathcal{N}_{CB}^{(\xi)}(t) = \sum_{j \in \text{CB}} |\beta_j^{(\xi)}(t)|^2. \quad (19)$$

Then, we define the final valley polarization of the graphene nanoring. To better characterize the asymmetry in valley populations of the system, we introduce two different expressions for the valley polarization. In the first expression, the valley polarization is defined as the difference between the CB populations of different valleys,

$$P = \frac{\mathcal{N}_{CB}^{(K)}(t = \infty) - \mathcal{N}_{CB}^{(K')}(t = \infty)}{\pi(R_{\text{out}}^2 - R_{\text{in}}^2)}, \quad (20)$$

where the valley polarization is defined per unit area of the nanoring.

The second expression defines the normalized valley polarization,

$$P_N = \frac{\mathcal{N}_{CB}^{(K)}(t = \infty) - \mathcal{N}_{CB}^{(K')}(t = \infty)}{\mathcal{N}_{CB}^{(K)}(t = \infty) + \mathcal{N}_{CB}^{(K')}(t = \infty)}. \quad (21)$$

This expression determines the fraction of the excited electrons, which occupy the two valleys differently. The maximum

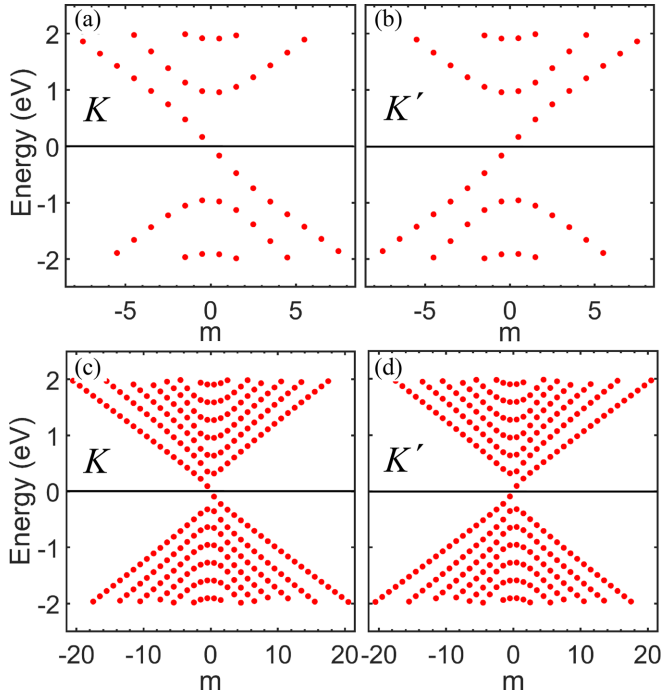


FIG. 1. Energy spectra of a graphene nanoring. The spectra are shown as a function of the magnetic quantum number  $m$ , which takes half-integer values. The size of the nanoring is  $R_{\text{in}} = 5$  nm,  $R_{\text{out}} = 15$  nm in (a) and (b) and  $R_{\text{in}} = 5$  nm,  $R_{\text{out}} = 35$  nm in (c) and (d). The spectra are shown (a) and (c) for the  $K$  valley and (b) and (d) for the  $K'$  valley.

value of  $P_N$  is 1, corresponding to the condition that all electrons are excited in only one valley.

### III. RESULTS AND DISCUSSION

The energy spectrum of the graphene nanoring, obtained from Eq. (9), is shown in Fig. 1 for both the  $K$  and  $K'$  valleys. It satisfies the condition of the time-reversal symmetry, i.e.,  $E_{K,m} = E_{K',-m}$ . The energy spectrum also has the following specific structure. It has a finite bulk band gap, which is due to the finite size of the system. Here, the states with positive energies belong to the conduction band, while the states with negative energies belong to the valence band. As expected, the band gap decreases with increasing the system's size. For example, for outer radius  $R_{\text{out}} = 15$  nm [see Figs. 1(a) and 1(b)] the band gap is around 2 eV, while for outer radius  $R_{\text{out}} = 35$  nm [see Figs. 1(c) and 1(d)] the band gap is 0.5 eV.

In addition to the gapped structure of the energy spectrum, there is a clear in-gap branch visible for each valley. These two branches are due to the edge states of the system [46–48]. The branches have different behaviors for the  $K$  and  $K'$  valleys. While for the  $K$  valley, the energy of the in-gap states decreases with the quantum number  $m$ , for the  $K'$  valley, the energy increases with  $m$ . Such fundamentally different behaviors of the energy spectrum at the two valleys result in different responses of the valley to a circularly polarized pulse. This is due to the fact that, for example, for a clockwise circularly polarized pulse, the dipole selection rule is  $m_{\text{final}} = m_{\text{initial}} + 1$ . Then, the rate of the optical transition

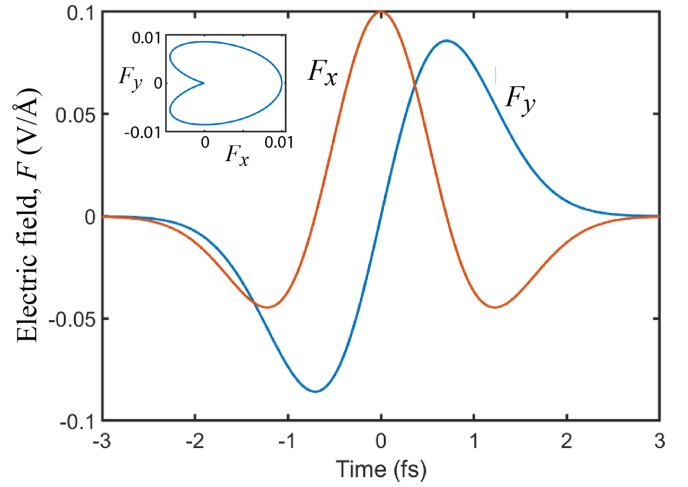


FIG. 2. Profile of the electric field of a left circularly polarized optical pulse. The pulse has only one oscillation. The amplitude of the pulse is  $F_0 = 0.1$  V/Å. The optical field has both  $x$  and  $y$  components. The inset shows the corresponding cycle of the optical pulse.

between the states is determined by the corresponding energy difference,  $\Delta E = E_{m_{\text{final}}} - E_{m_{\text{initial}}}$ . The value of  $\Delta E$  is different for the  $K$  and  $K'$  valleys, which finally results in different after-the-pulse CB populations for the two valleys.

As mentioned above, the continuous model of graphene generates an infinite number of states within the nanoring. In Fig. 1, we show only the energy levels taken into account in our calculations. These levels are within the energy window  $-2$  eV  $< E < 2$  eV. Such an energy interval is chosen in such a way that for the optical pulse with an amplitude up to  $F_0 = 0.3$  eV, the valley polarization converges to the values presented below with accuracy less than 5%.

We apply a single cycle of a left circularly polarized optical pulse. The pulse profile, i.e., the  $x$  and  $y$  components of the pulse electric field, is shown in Fig. 2. Before the pulse, all states of graphene nanoring with negative energies are populated. The optical pulse results in the redistribution of electrons between the states of the nanoring and in the population of the CB states, both the in-gap states and the bulk states.

One of the main characteristics of electron dynamics in the field of the pulse is the total CB population  $\mathcal{N}_{CB}^{(\xi)}$ . In Fig. 3, the CB population is shown as a function of time for the two valleys,  $K$  and  $K'$ , and different amplitudes of the pulse  $F_0$ . The size of the nanoring is  $R_{\text{in}} = 5$  nm and  $R_{\text{out}} = 15$  nm. For all values of  $F_0$  the electron dynamics is highly irreversible; that is, the maximum CB population is almost the same as the final CB population, i.e., the population after the pulse. The irreversible dynamics has also been observed in the graphene monolayer [49]. Another essential property of CB population dynamics is that the final CB population for the  $K$  valley is always greater than the corresponding population for the  $K'$  valley. This means that, after the pulse, there is a finite valley polarization of the graphene nanoring.

As expected, the CB population monotonically increases with the field amplitude (see Fig. 3). Here, the results are shown for a frequency of the pulse around 1.0 eV, which

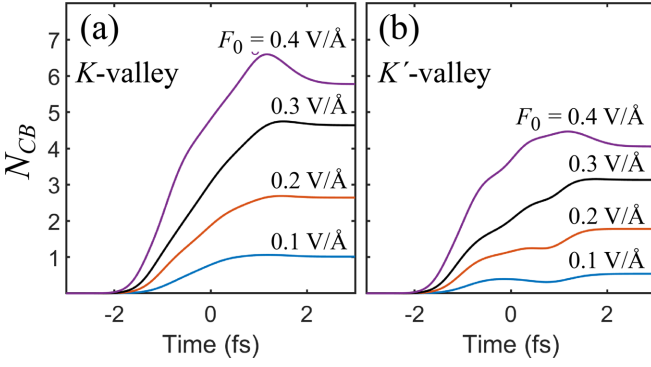


FIG. 3. Conduction band population as a function of time. The conduction band states are the states with positive energies. The data are shown for different field amplitudes for (a) the  $K$  valley and (b) the  $K'$  valley. The corresponding values of  $F_0$  are shown next to each line. The inner and outer radii of the nanoring are  $R_{in} = 5$  nm,  $R_{out} = 15$  nm. The time constant, which determines the frequency and the duration of the optical pulse, is  $\tau = 1$  fs. The optical pulse is left circularly polarized.

corresponds to the time parameter of  $\tau = 1$  fs [see Eqs. (14) and (15)]. To illustrate the effect of the pulse frequency on the electron dynamics, we show in Fig. 4 the CB population for different values of  $\tau$ . In all cases, the pulse has only one oscillation. With increasing  $\tau$ , the pulse frequency decreases, which enhances the coupling of the VB states and the in-gap CB states, where the energy separation between them is relatively small, i.e., less than 1 eV. As a result, the populations of the in-gap edge states increase with  $\tau$ . Such a tendency is visible in Fig. 4 for both valleys, while it is more pronounced for the  $K$  valley.

To characterize the final state of the electron system, we show in Fig. 5 the occupations of individual CB levels after the pulse. The results are shown for different field amplitudes. As discussed above, with increasing the field amplitude  $F_0$ , the

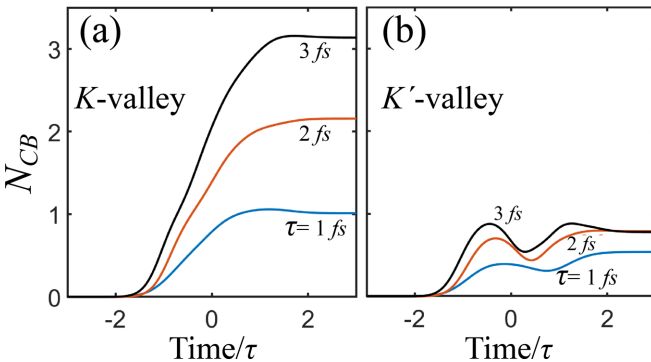


FIG. 4. Conduction band population as a function of time. The conduction band states are the states with positive energy. The data are shown for different values of parameter  $\tau$  for (a) the  $K$  valley and (b) the  $K'$  valley. The corresponding values of  $\tau$  are shown next to each line. Parameter  $\tau$  determines both the frequency of the pulse and its duration. The time is shown in dimensionless units,  $t/\tau$ . The inner and outer radii of the nanoring are  $R_{in} = 5$  nm and  $R_{out} = 15$  nm. The field amplitude is  $F_0 = 0.1$  V/Å. The optical pulse is left circularly polarized.

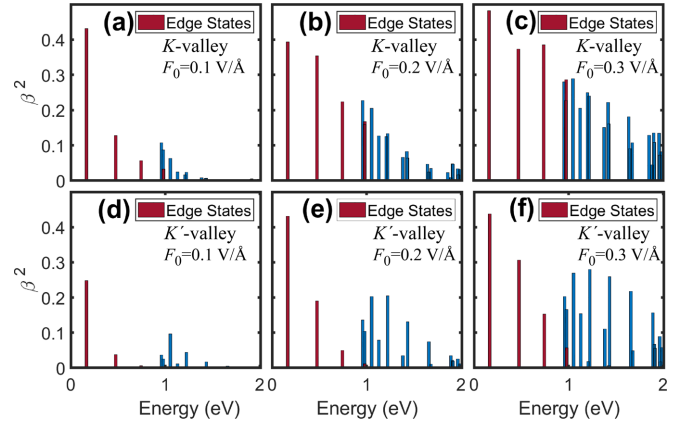


FIG. 5. Population of individual conduction band levels. The results are for (a)–(c) the  $K$  valley and (d)–(f) the  $K'$  valley. The amplitude of the pulse is  $F_0 = 0.1$  V/Å in (a) and (d),  $F_0 = 0.2$  V/Å in (b) and (e), and  $F_0 = 0.3$  V/Å in (c) and (f). The inner and outer radii of the nanoring are  $R_{in} = 5$  nm and  $R_{out} = 15$  nm. The red lines correspond to in-gap edge states, while the blue lines correspond to bulk states of the nanoring. The time constant of the pulse is  $\tau = 1$  fs. The optical pulse is left circularly polarized.

occupations of the CB levels monotonically increase, which occurs for each level. At the same time, the largest occupations are visible for the in-gap edge CB states, which are marked by red lines. Also, the main difference between the  $K$  and  $K'$  valleys is mainly in the populations of the in-gap edge states. For example, comparing Figs. 5(c) and 5(f), we can say that the populations of the bulk CB states, which are shown by blue lines, are almost the same for the  $K$  and  $K'$  valleys, while the populations of the edge CB states (red lines) are quite different. This difference results in the final valley polarization of the system.

To emphasize the effect of the frequency of the pulse on the ultrafast electron dynamics, we show in Fig. 6 the final populations of the CB levels for different values of  $\tau$ . When the time parameter  $\tau$  increases from 1 to 2 fs, the populations of the in-gap edge states are strongly increased. This is because the pulse frequency becomes smaller, and the low-energy CB states become more populated. Such an enhancement is more pronounced for the  $K$  valley (see Fig. 6). For example, the populations of all edge CB states (the red lines in Fig. 6) strongly increase when  $\tau$  changes from 1 to 2 fs for the  $K$  valley, and almost all of them become around 0.4, while for the  $K'$  valley, even for  $\tau = 2$  fs, only two red lines are visible, with populations of 0.4 and 0.1.

The main outcome of the interaction of the circularly polarized pulse with the graphene nanoring is the valley polarization of the electron system. We have used two expressions to define the valley polarization,  $P$  and  $P_N$  [see Eqs. (20) and (21)]. Here,  $P$  is just the difference between the CB populations of the  $K$  and  $K'$  valleys per unit area, while  $P_N$  is its normalized value.

In Fig. 7, the valley polarization  $P$  is shown as a function of the field amplitude for different parameters of the nanoring. At small field amplitudes, the valley polarization quadratically increases with  $F_0$ . At large values of  $F_0$ , the valley polarization shows a saturated behavior. Such saturation is related to the

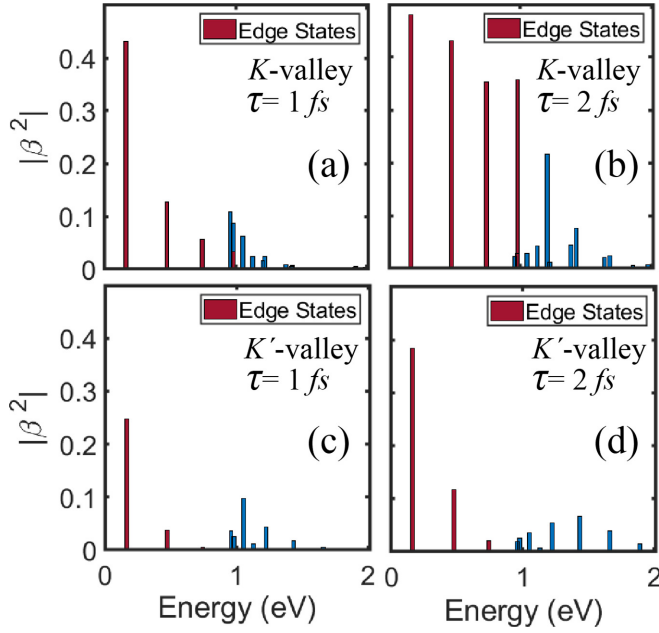


FIG. 6. Population of individual conduction band levels. The results are for (a) and (b) the  $K$  valley and (c) and (d) the  $K'$  valley. The time constant of the optical pulse is  $\tau = 1$  fs in (a) and (c) and  $\tau = 2$  fs in (b) and (d). The inner and outer radii of the nanoring are  $R_{in} = 5$  nm and  $R_{out} = 15$  nm. The red lines correspond to in-gap edge states, while the blue lines correspond to bulk states of the nanoring. The amplitude of the pulse is  $F_0 = 0.1$  V/Å. The optical pulse is left circularly polarized.

finite number of nanoring levels considered in the model. Although our results are the most accurate for a field amplitude less than  $0.3$  V/Å, we show the data for field amplitudes up to  $0.5$  V/Å to illustrate the effect of a finite number of levels within a nanoscale system.

In Fig. 7(a), the inner radius of the nanoring is fixed, and the outer radius is varied. The results show that with increasing the outer radius, the valley polarization  $P$ , defined as the polarization per unit area, decreases. This is consistent with the fact that the valley polarization of the graphene monolayer, i.e., an infinite graphene nanoring, is zero.

Figure 7(b) illustrates the valley polarization's dependence on the nanoring's inner radius. In this case, with decreasing the inner radius, while the size of the nanoring increases, the valley polarization still increases. Thus, these results suggest that the maximum valley polarization is achieved for a nanoring with the smallest inner radius, i.e., for a disk. To check this statement, we calculated the valley polarization for a disk using the infinite mass boundary conditions at the disk's boundary. The results show that for a graphene disk with a radius of  $15$  nm, the valley polarization is  $P = 0.0028$  nm $^{-2}$  for a field amplitude of  $0.2$  V/Å, while for a ring with an inner radius of  $5$  nm and an outer radius of  $15$  nm, the corresponding valley polarization has a smaller value,  $P = 0.0014$  nm $^{-2}$ . These data support the above statement that the valley polarization is the largest for the disk. A detailed analysis of the valley polarization generated in graphene nanodisks by the optical pulse will be given elsewhere.

At small field amplitudes  $F_0$ , the valley polarization has a quadratic dependence on  $F_0$ , i.e., a linear dependence on

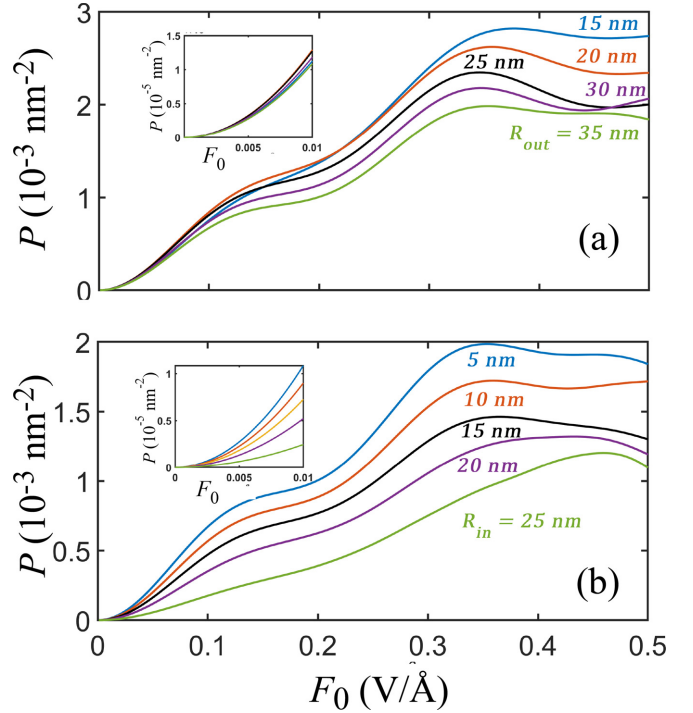


FIG. 7. The valley polarization of a graphene nanoring. The valley polarization is defined by Eq. (20) and is shown as a function of the field amplitude  $F_0$  for different parameters of the nanoring. In (a), the inner radius is fixed at  $R_{in} = 5$  nm, and the outer radius is varied with the corresponding values shown next to each line. In (b), the outer radius is fixed at  $R_{out} = 35$  nm, and the inner radius is varied with the corresponding values shown next to each line. The time constant of the pulse is  $\tau = 1$  fs, and the pulse is left circularly polarized. The insets in each panel show the valley polarization at small values of  $F_0$ .

the power of the pulse, with a coefficient that depends on the parameters of the nanoring. We can approximate this dependence with the following expression:

$$P = \frac{5.42R_{out} - 5.89R_{in} + 30}{R_{out}^2 - R_{in}^2} F_0^2, \quad (22)$$

where  $F_0$  is measured in volts per angstrom and  $R_{out}$  and  $R_{in}$  are in nanometers. Equation (22) can be used to design the nanoring with a given value of the valley polarization.

The valley polarization can also be characterized by its normalized value [see Eq. (21)], which shows the fraction of the excited electrons that are valley polarized. The normalized valley polarization as a function of the field amplitude  $F_0$  is shown in Fig. 8 for different sizes of the nanoring. Similar to the case of valley polarization  $P$  (see Fig. 7), for a fixed internal radius of the nanoring  $R_{in}$ , the valley polarization  $P_N$  decreases with increasing the size of the system, i.e.,  $R_{out}$  [see Fig. 8(b)]. This is consistent with the expectation that with increasing the size of the nanoring, the system becomes more similar to a pristine graphene monolayer, for which there is no valley polarization after a circularly polarized pulse.

Also, when the outer radius is fixed and the inner radius is varied [see Fig. 8(a)], the valley polarization increases with decreasing the inner radius of the nanoring  $R_{in}$ . This behavior

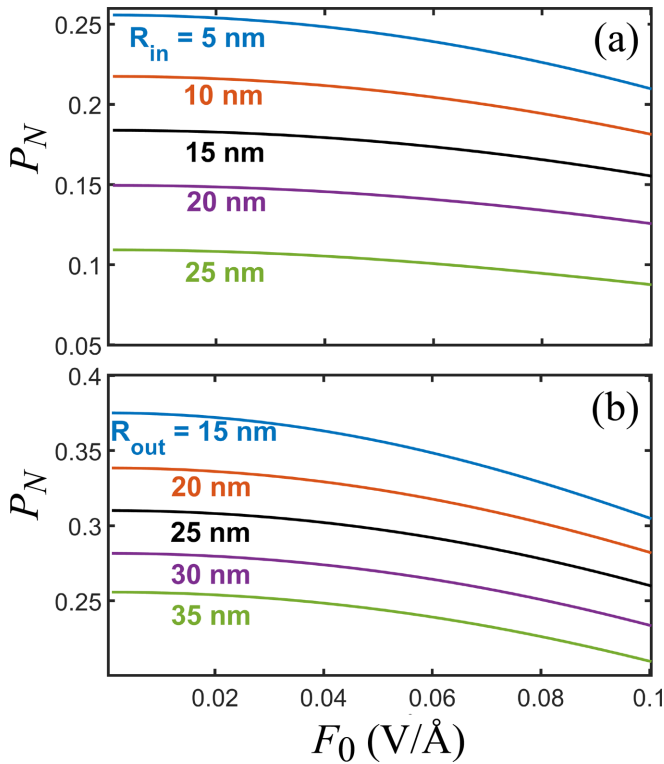


FIG. 8. The valley polarization of a graphene nanoring. The valley polarization is defined by Eq. (21) and is shown as a function of the field amplitude  $F_0$  for different parameters of the nanoring. In (a), the outer radius is fixed at  $R_{\text{out}} = 35$  nm, and the inner radius is varied with the corresponding values shown next to each line. In (b), the inner radius is fixed at  $R_{\text{in}} = 5$  nm, and the outer radius is varied with the corresponding values shown next to each line. The time constant of the pulse is  $\tau = 1$  fs, and the pulse is left circularly polarized.

is similar to what was shown in Fig. 7(b) and also means that the maximum valley polarization is observed for a small inner radius. The normalized valley polarization can reach a value of up to 40% [see Fig. 8(b)].

The main difference between the valley polarizations  $P$  and  $P_N$  is that, at small field amplitudes, the normalized valley polarization almost does not depend on the field amplitude. Its dependence on the parameters of the nanoring can be approximated by the following expression:

$$P_N = -0.005886R_{\text{out}} - 0.0072R_{\text{in}} + 0.4964. \quad (23)$$

This expression can be used to predict the valley polarization for a nanoring of a given size.

Comparing the behaviors of  $P$  and  $P_N$ , we can see that, at a finite field amplitude  $F_0$ ,  $P$  increases with  $F_0$ , while  $P_N$  decreases. For the valley polarization  $P$ , its increase with  $F_0$  is because, at larger field amplitudes, more nanoring levels are excited, resulting in larger populations of both the  $K$  and  $K'$  valleys and, correspondingly, in larger valley polarization  $P$ . For the valley polarization  $P_N$ , which is defined as a fraction of excited electrons that are valley polarized, both the number of excited electrons and the difference between the CB

populations of the two valleys increase with  $F_0$ . The main contribution to the difference in the CB populations of the valleys comes from the edge states, while the total population of the CB is determined by both the edge states and the bulk states of the nanoring. As a result, the valley polarization  $P_N$  decreases with increasing the field amplitude.

Expressions (22) and (23) have been obtained for a particular profile of the optical pulse, which is a single oscillation circularly polarized optical pulse with a time constant of  $\tau = 1$  fs. Similar expressions can be obtained for optical pulses of different polarizations, frequencies, and durations. The parameters of the edge states of the graphene nanoring depend on the shape of the ring and the model used to describe it [47]. Thus, they will also affect the valley polarization and the corresponding expressions (22) and (23).

#### IV. CONCLUSION

In graphenelike systems with two valleys, the valley polarization can be induced only through processes which break the time-reversal symmetry. For example, such polarization can be introduced in systems interacting with a circularly polarized pulse. Here, ultrashort optical pulses are particularly interesting since they allow control of the valley degree of freedom on a femtosecond timescale. The valley polarization can be induced by such an ultrashort circularly polarized pulse in monolayers of graphenelike materials only if they have broken inversion symmetry. The broken inversion symmetry also introduces a finite band gap in the system. Thus, in pristine graphene, which has inversion symmetry, no valley polarization can be generated by any short optical pulse. To resolve this problem, we considered a graphene monolayer with broken translational symmetry, i.e., a graphene nanoring. The energy spectrum of such a nanoring consists of bulk states with a finite band gap between the valence and conduction bands and in-gap edge states. Such in-gap states are mainly responsible for generating the finite valley polarization of the nanoring. The valley polarization induced by the ultrashort optical pulse depends on the parameters of the nanoring, i.e., its inner and outer radii. With increasing the size of the nanoring, the normalized valley polarization decreases and converges to a zero value for the infinite graphene monolayer.

Although we considered a particular shape of the graphene nanosystem, i.e., a nanoring, we expect that the valley polarization can be induced by an ultrashort circularly polarized pulse for a graphene nanoflake of any shape. In our analysis, we also did not consider intervalley mixing induced by the boundaries of the graphene nanosystem. Such mixing can be significant only for relatively small graphene nanorings.

#### ACKNOWLEDGMENTS

Major funding was provided by Grant No. DE-FG02-01ER15213 from the Chemical Sciences, Biosciences, and Geosciences Division, Office of Basic Energy Sciences, Office of Science, U.S. Department of Energy. Numerical simulations were performed using support from Grant No. DE-SC0007043 from the Materials Sciences and Engineering Division of the Office of the Basic Energy Sciences, Office of Science, U.S. Department of Energy.

- [1] P. R. Wallace, The band theory of graphite, *Phys. Rev.* **71**, 622 (1947).
- [2] K. S. Novoselov, A. K. Geim, S. V. Morozov, D. Jiang, Y. Zhang, S. V. Dubonos, I. V. Grigorieva, and A. A. Firsov, Electric field effect in atomically thin carbon films, *Science* **306**, 666 (2004).
- [3] A. K. Geim and K. S. Novoselov, The rise of graphene, *Nat. Mater.* **6**, 183 (2007).
- [4] A. H. Castro Neto, F. Guinea, N. M. R. Peres, K. S. Novoselov, and A. K. Geim, The electronic properties of graphene, *Rev. Mod. Phys.* **81**, 109 (2009).
- [5] D. S. L. Abergel, V. Apalkov, J. Berashevich, K. Ziegler, and T. Chakraborty, Properties of graphene: A theoretical perspective, *Adv. Phys.* **59**, 261 (2010).
- [6] S. Das Sarma, S. Adam, E. H. Hwang, and E. Rossi, Electronic transport in two-dimensional graphene, *Rev. Mod. Phys.* **83**, 407 (2011).
- [7] A. F. Young and P. Kim, Electronic transport in graphene heterostructures, *Annu. Rev. Condens. Matter Phys.* **2**, 101 (2011).
- [8] D. Xiao, M. C. Chang, and Q. Niu, Berry phase effects on electronic properties, *Rev. Mod. Phys.* **82**, 1959 (2010).
- [9] J. R. Schaibley, H. Yu, G. Clark, P. Rivera, J. S. Ross, K. L. Seyler, W. Yao, and X. Xu, Valleytronics in 2d materials, *Nat. Rev. Mater.* **1**, 16055 (2016).
- [10] J. Schaibley, Valleytronics in 2D semiconductors, in *2D Materials for Photonic and Optoelectronic Applications*, edited by Q. Bao and H. Y. Hoh (Woodhead, Amsterdam, 2020), pp. 281–302.
- [11] S. A. Vitale, D. Nezich, J. O. Varghese, P. Kim, N. Gedik, P. Jarillo-Herrero, D. Xiao, and M. Rothschild, Valleytronics: Opportunities, challenges, and paths forward, *Small* **14**, 1801483 (2018).
- [12] H. K. Kelardeh, V. Apalkov, and M. I. Stockman, Attosecond strong-field interferometry in graphene: Chirality, singularity, and Berry phase, *Phys. Rev. B* **93**, 155434 (2016).
- [13] S. A. Oliaei Motlagh, J.-S. Wu, V. Apalkov, and M. I. Stockman, Femtosecond valley polarization and topological resonances in transition metal dichalcogenides, *Phys. Rev. B* **98**, 081406(R) (2018).
- [14] S. A. Oliaei Motlagh, F. Nematollahi, V. Apalkov, and M. I. Stockman, Topological resonance and single-optical-cycle valley polarization in gapped graphene, *Phys. Rev. B* **100**, 115431 (2019).
- [15] K. Rana Magar, A. Oliaei Motlagh, and V. Apalkov, Topological resonance in graphene-like materials, *J. Phys. Condens. Matter* **34**, 375301 (2022).
- [16] O. Wang, K. Kalantar-Zadeh, A. Kis, J. N. Coleman, and M. S. Strano, Electronics and optoelectronics of two-dimensional transition metal dichalcogenides, *Nat. Nanotechnol.* **7**, 699 (2012).
- [17] K. S. Novoselov, A. Mishchenko, A. Carvalho, and A. H. Castro Neto, 2D materials and van der Waals heterostructures, *Science* **353**, aac9439 (2016).
- [18] J. W. Jiang, Graphene versus MoS<sub>2</sub>: A short review, *Front. Phys.* **10**, 287 (2015).
- [19] M. Ezawa, Photoinduced Topological Phase Transition and a Single Dirac-Cone State in Silicene, *Phys. Rev. Lett.* **110**, 026603 (2013).
- [20] H. Oughaddou, H. Enriquez, M. R. Tchalala, H. Yildirim, A. J. Mayne, A. Bendounan, G. Dujardin, M. Ait Ali, and A. Kara, Silicene, a promising new 2D material, *Prog. Surf. Sci.* **90**, 46 (2015).
- [21] J. Zhao, H. Liu, Z. Yu, R. Quhe, S. Zhou, Y. Wang, C. C. Liu, H. Zhong, N. Han, J. Lu, Y. Yao, and K. Wu, Rise of silicene: A competitive 2D material, *Prog. Mater. Sci.* **83**, 24 (2016).
- [22] D. Jariwala, A. Srivastava, and P. M. Ajayan, Graphene synthesis and band gap opening, *J. Nanosci. Nanotechnol.* **11**, 6621 (2011).
- [23] M. S. Nevius, M. Conrad, F. Wang, A. Celis, M. N. Nair, A. Taleb-Ibrahimi, A. Tejada, and E. H. Conrad, Semiconducting Graphene from Highly Ordered Substrate Interactions, *Phys. Rev. Lett.* **115**, 136802 (2015).
- [24] D. Pan, J. Zhang, Z. Li, and M. Wu, Hydrothermal route for cutting graphene sheets into blue-luminescent graphene quantum dots, *Adv. Mater.* **22**, 734 (2010).
- [25] S.-Y. Li and L. He, Recent progresses of quantum confinement in graphene quantum dots, *Front. Phys.* **17**, 33201 (2022).
- [26] G. Y. Wu, N. Y. Lue, and L. Chang, Graphene quantum dots for valley-based quantum computing: A feasibility study, *Phys. Rev. B* **84**, 195463 (2011).
- [27] T. Chakraborty, F. Peeters, and U. Sivan, *Nano-Physics and Bio-Electronics A New Odyssey* (Elsevier, Amsterdam, 2002).
- [28] R. C. Ashoori, Electrons in artificial atoms, *Nature (London)* **379**, 413 (1996).
- [29] T. Chakraborty, *Quantum Dots* (Elsevier, Amsterdam, 1999).
- [30] S. M. Reimann and M. Manninen, Electronic structure of quantum dots, *Rev. Mod. Phys.* **74**, 1283 (2002).
- [31] T. A. Fulton and G. J. Dolan, Observation of Single-Electron Charging Effects in Small Tunnel Junctions, *Phys. Rev. Lett.* **59**, 109 (1987).
- [32] L. Kouwenhoven and L. Glazman, Revival of the Kondo effect, *Phys. World* **14**, 33 (2001).
- [33] Y. Arakawa and H. Sakaki, Multidimensional Quantum Well Laser and Temperature Dependence of its Threshold Current, *Appl. Phys. Lett.* **40**, 939 (1982).
- [34] D. Loss and D. P. DiVincenzo, Quantum computation with quantum dots, *Phys. Rev. A* **57**, 120 (1998).
- [35] X. Michalet, F. F. Pinaud, L. A. Bentolila, J. M. Tsay, S. Doose, J. J. Li, G. Sundaresan, A. M. Wu, S. S. Gambhir, and S. Weiss, Quantum dots for live cells, in vivo imaging, and diagnostics, *Science* **307**, 538 (2005).
- [36] V. Veeramani, Z. Bao, M.-H. Chan, H.-C. Wang, A. Jena, H. Chang, S.-F. Hu, and R.-S. Liu, Quantum dots for light conversion, therapeutic and energy storage applications, *J. Solid State Chem.* **270**, 71 (2019).
- [37] Q. Liu, J. Sun, K. Gao, N. Chen, X. Sun, D. Ti, C. Bai, R. Cui, and L. Qu, Graphene quantum dots for energy storage and conversion: From fabrication to applications, *Mater. Chem. Front.* **4**, 421 (2020).
- [38] M. V. Berry and R. J. Mondragon, Neutrino billiards: Time-reversal symmetry-breaking without magnetic fields, *Proc. R. Soc. London, Ser. A* **412**, 53 (1987).
- [39] S. Schnez, K. Ensslin, M. Sigrist, and T. Ihn, Analytic model of the energy spectrum of a graphene quantum dot in a perpendicular magnetic field, *Phys. Rev. B* **78**, 195427 (2008).
- [40] M. Grujic, M. Zarenia, A. Chaves, M. Tadić, G. A. Farias, and F. M. Peeters, Electronic and optical properties of a circular graphene quantum dot in a magnetic field: Influence of the boundary conditions, *Phys. Rev. B* **84**, 205441 (2011).



- [41] M. R. Thomsen and T. G. Pedersen, Analytical Dirac model of graphene rings, dots, and antidots in magnetic fields, *Phys. Rev. B* **95**, 235427 (2017).
- [42] L. A. Ponomarenko, F. Schedin, M. I. Katsnelson, R. Yang, E. W. Hill, K. S. Novoselov, and A. K. Geim, Chaotic Dirac billiard in graphene quantum dots, *Science* **320**, 356 (2008).
- [43] J. Eroms and D. Weiss, Weak localization and transport gap in graphene antidot lattices, *New J. Phys.* **11**, 095021 (2009).
- [44] Q. Xu, M.-Y. Wu, G. F. Schneider, L. Houben, S. K. Malladi, C. Dekker, E. Yucelen, R. E. Dunin-Borkowski, and H. W. Zandbergen, Controllable atomic scale patterning of freestanding monolayer graphene at elevated temperature, *ACS Nano* **7**, 1566 (2013).
- [45] A. J. M. Giesbers, E. C. Peters, M. Burghard, and K. Kern, Charge transport gap in graphene antidot lattices, *Phys. Rev. B* **86**, 045445 (2012).
- [46] D. A. Bahamon, A. L. C. Pereira, and P. A. Schulz, Inner and outer edge states in graphene rings: A numerical investigation, *Phys. Rev. B* **79**, 125414 (2009).
- [47] D. R. da Costa, A. Chaves, M. Zarenia, J. M. Pereira, G. A. Farias, and F. M. Peeters, Geometry and edge effects on the energy levels of graphene quantum rings: A comparison between tight-binding and simplified Dirac models, *Phys. Rev. B* **89**, 075418 (2014).
- [48] Q. Zhang, T. C. Wu, G. Kuang, A. Xie, and N. Lin, Investigation of edge states in artificial graphene nano-flakes, *J. Phys.: Condens. Matter* **33**, 225003 (2021).
- [49] H. K. Kelardeh, V. Apalkov, and M. I. Stockman, Graphene in ultrafast and superstrong laser fields, *Phys. Rev. B* **91**, 045439 (2015).